that actually occurred. Furthermore, the native feldspar grains collected from uncontaminated regions of the aquifer showed little evidence of chemical weathering, consistent with the expected inorganic dissolution rate (*10*).

Bacteria were located at or near the etch pits. The etch pits, however, are not at the actual contact surface of the microbes, and the distinctive shape and extent of etching suggest that the mineral surface is in contact with an aqueous weathering fluid. We postulate that surface-adhering bacteria created a reaction zone in their immediate vicinity in which organic acids, produced within the cell and released extracellularly, were concentrated at the cell solution–mineral interface (Fig. 3). During metabolism, organic substrate was consumed by heterotrophic bacteria, whereas enzymes and metabolic by-products such as organic acids were exported from the cell interior to the nearby fluid environment. A gradient in chemical potential was produced between the cell surface and the surrounding bulk fluid. High concentrations of these by-products may be present in the near vicinity of the microorganisms. Within this microenvironment, complex organic acids chelated SiO_2 at the quartz surface and dissolved the mineral even though the bulk pore water was supersaturated with respect to the dissolving mineral. Silica, and possibly alumina, thus chelated and in solution, is available for transport away from the dissolution site along the ground-water flow path.

The activity of indigenous microorganisms may represent a previously overlooked factor in modeling subsurface geochemistry. In addition, those geochemical processes reported may represent an alternative mechanism for the generation of secondary porosity in low-temperature (up to 70°C) sedimentary basins.

REFERENCES AND NOTES

1. E. K. Berner and R. A. Berner, *The Global Water Cycle, Geochemistry and Environment* (Prentice-Hall, Englewood Cliffs, NJ, 1987), pp. 148–165.
2. W. H. Huang and W. D. Keller, *Am. Mineral.* **55**, 2076 (1970); J. Schott, R. L. Berner, E. L. Sjoberg, *Geochim. Cosmochim. Acta* **45**, 2123 (1981); L. Chou and R. Wollast, *Am. J. Sci.* **285**, 963 (1985); G. R. Holdren and P. M. Speyer, *ibid.*, p. 994; K. G. Knauss and T. J. Wolery, *Geochim. Cosmochim. Acta* **50**, 2481 (1986); M. A. Mast and J. I. Drever, *ibid.* **51**, 2559 (1987).
3. P. C. Bennett, D. I. Siegel, *Nature* **326**, 684 (1987).
4. _____, B. M. Hill, P. H. Glaser, *Geology* **19**, 328 (1991).
5. W. Stumm and G. Furrer, in *Aquatic Surface Chemistry*, W. Stumm, Ed. (Wiley, New York, 1987), chap. 8.
6. P. C. Bennett, *Geochim. Cosmochim. Acta* **55**, 1781 (1991).
7. D. L. Balkwill and W. C. Ghiorse, *Appl. Environ. Microbiol.* **50**, 580 (1985); W. C. Ghiorse and J. T. Wilson, *Adv. Appl. Microbiol.* **33**, 107 (1988); E. L. Madsen, J. L. Sinclair, W. C. Ghiorse, *Science* **252**, 830 (1991); R. M. Atlas, Ed., *Petroleum Microbiology* (Macmillan, New York, 1984).
8. I. M. Cozzarelli, R. P. Eganhouse, M. J. Baedecker, *Environ. Geol. Water Sci.* **16**, 135 (1990).
9. Exceptions include F. H. Chapelle and D. R. Lovley, *Appl. Environ. Microbiol.* **56**, 1865 (1990); F. H. Chapelle and P. B. McMahon, *J. Hydrol.* **127**, 85 (1991); P. B. McMahon and F. H. Chapelle, *Nature* **349**, 233 (1991); _____, W. F. Falls, P. M. Bradley, *J. Sediment. Petrol.* **62**, 1 (1992).
10. M. J. Baedacker, D. I. Siegal, P. C. Bennett, I. M. Cozzarelli, *U.S. Geol. Surv. Water Res. Invest. Rep. 88-4220* (1989); M. J. Baedecker, I. M. Cozzarelli, P. C. Bennett, D. I. Siegel, in preparation.
11. F. H. Chang and G. Ehrlich, *U.S. Geol. Surv. Water Res. Invest. Rep. 84-4188* (1984).
12. Minerals were obtained from Wards Natural Science Establishment, Inc., albite 46E0230, -2 and -4; quartz 46E6605, -7 and -9; anorthite 46E0555, -7 and -9; and anorthoclase 46E0575, -7 and -9.
13. During the preparation of the mineral materials for these experiments, not all phases were carried out under strictly sterile conditions. However, standard techniques for the aseptic handling of microbial cultures and of sterile materials were used, and every effort was made to minimize the possibility of contamination of the mineral specimens by opportunistic microorganisms. Examination of mineral grains reserved as controls has not shown any evidence of microbial contamination.
14. J. W. Costerton, in *Adsorption of Microorganisms to Surfaces*, G. Bitton and K. C. Marshall, Eds. (Wiley, New York, 1980), chap. 12.
15. F. K. Hiebert, R. L. Folk, P. C. Bennett, C. H. Oppenheimer, L. W. Lake, *Eos* **71**, 503 (1990).
16. R. A. Berner and G. R. Holdren, Jr., *Geochim. Cosmochim. Acta* **43**, 1173 (1979); _____, J. Schott, *ibid.* **49**, 1657 (1985).

17. We thank R. L. Folk, M. J. Baedecker, I. M. Cozzarelli, D. I. Siegel, L. Crossey, and J. Horowitz. Supported by the National Science Foundation, the U.S. Geological Survey, and the Geology Foundation of The University of Texas at Austin.

20 May 1992; accepted 4 August 1992

Fault Zone Connectivity: Slip Rates on Faults in the San Francisco Bay Area, California

Roger Bilham and Paul Bodin

The slip rate of a fault segment is related to the length of the fault zone of which it is part. In turn, the slip rate of a fault zone is related to its connectivity with adjoining or contiguous fault zones. The observed variation in slip rate on fault segments in the San Francisco Bay area in California is consistent with connectivity between the Hayward, Calaveras, and San Andreas fault zones. Slip rates on the southern Hayward fault taper northward from a maximum of more than 10 millimeters per year and are sensitive to the active length of the Maacama fault.

The mean recurrence interval between damaging earthquakes on a fault is determined in part by its slip rate (*1*). Slip rate data are obtained by summing the moments of historic earthquakes (*2*) or by direct observation of the offset rate of geological features (*3*). Historic summations of seismic moment are inaccurate where the instrumental or written record endures for fewer than several earthquake cycles, as in California. Moreover, exhumation of faults to learn their historic slip rates can result in inaccurate estimates of slip rate at seismogenic depths because slip may be distributed over a wide region. For example, no surface evidence for fault slip exists for the inferred 1.8 m of dextral slip that accompanied the 1989 Loma Prieta earthquake (*4*), and slip on the nearby San Andreas fault during the 1906 San Francisco earthquake was significantly underestimated by observed fault offsets (*5*). Relative plate motion between the Pacific and North American plates is distributed principally among faults of the San Andreas system, a branching network of interconnected fault zones (*6*). Although detailed geodetic studies show the distribution of velocities across the plate boundary, these data do not contribute to our understanding of long-term slip rates on mapped faults. The observed deformation field may be generated by several plausible but non-unique distributions of slip on faults in the plate boundary (*7*). In this report we examine an alternative method to estimate the relative slip rates of faults in a complex plate boundary based on the geometry and mechanical linkage of mapped faults. In our proposed model we assume that the long-term slip rates of faults are determined by their current and evolving geometries.

For a wide range of fault lengths, the total geologic offset of a fault zone increases with fault zone length (*8*). Total offset is a maximum near the center of the fault zone and decays to small values near its ends. Similarly, the coseismic slip on an individual rupture increases with rupture length (*9*) and decays to zero at the ends of the rupture. Slip amplitude and distribution are influenced by the strain at failure (*10*), the geometry of the fault (*11, 12*), and the aspect ratio of the rupture surface (*13*). Earthquakes seldom rupture an entire fault zone. Instead they rupture segments or groups of segments that together result in the observed total offset of faults (*14*). As a result (Fig. 1), the slip rate of a segmented

Cooperative Institute for Research in the Environmental Sciences and Department of Geological Sciences, University of Colorado, Boulder, CO 80309–0216.

fault zone has a maximum near its center and its mean slip rate is proportional to its length for a given strain at failure. The calculations in Fig. 1 apply to the release of elastic strain, and it is clear that inelastic deformation must be responsible for the observed total geologic slip of many fault zones (*15*). However, we assume that this inelastic deformation is driven by stress geometries similar to those accompanying elastic models.

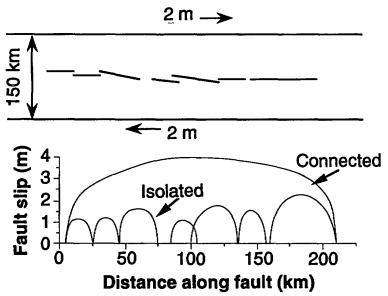

Fig. 1. Fault segments subjected to an applied shear strain (27 microstrain, in this case) slip less in isolation than when connected. Rupture of a fault zone typically occurs in earthquakes that rupture one or more contiguous segments, which release a fraction of the total slip proportional to the rupture of the entire fault zone. It follows that more earthquakes of a given size must occur near the center of the fault zone and thus that the slip rate is higher there than near the ends where the fault is pinned. Slip was calculated from a boundary element model of an elastic plate subject to antisymmetric displacements parallel to the mean strike of the fault (*11*).

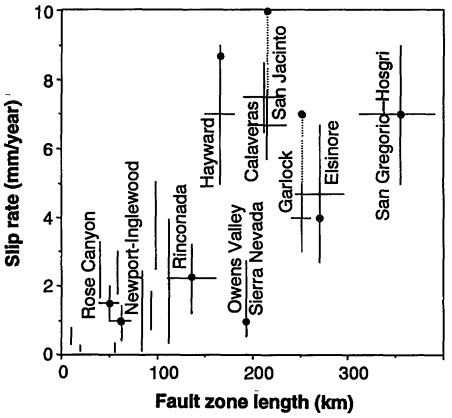

Fig. 2. Slip rate as a function of fault zone length in California. Vertical error bars indicate mean fault zone slip rate from published compilations (*1, 16, 29, 30*), weighted according to the fractional length of the fault zone to which the observations apply. Filled circles indicate mean slip rates adopted in conservative seismic hazard studies (*16*). Vertical lines indicate slip rates for faults in the Los Angeles Basin (*31*). There is no general consensus on the length or slip rate appropriate for the San Gregorio–Hosgri fault zone. Models developed in this report suggest that the mean slip rate may be less than 4 mm/year.

Slip rate data on California fault zones are consistent with this inferred relation between slip rate and fault zone length (Fig. 2). For example, slip rates approach a maximum near the center of the San Jacinto fault zone and are a minimum near each end (*16*). We conclude from Fig. 2 that it may be possible to estimate the slip rate of a fault segment where the effective fault zone length is known or the fault zone length where the distribution of slip rate is known. The first is important in estimating the recurrence time for earthquakes of a given size on a fault, and the second is of value in estimating the maximum possible length of earthquake rupture on a fault zone.

The nature of mechanical coupling between segments is irrelevant to this discussion, although recent investigations show that some faults are considerably simpler at depth than at surface (*17*). The connectivity we perceive may result from a ductile process below the seismogenic zone, a yield-point process at offsets between fault segments, or a distributed rupture process associated with occasional throughgoing rupture between segments. A difficulty arises, however, in quantifying this connectivity from fault geometry alone. For example, uncertainties in the lengths of fault zones shown in Fig. 2 arise from subjective decisions related to the inclusion of fault segments of questionable activity near the ends of fault zones. They also result from questions about whether to include subparallel fault segments, or other fault zones, that are significantly offset (>5 km) from the fault zone in question. The relation in Fig. 2 is perhaps surprising because it does not account for the interaction of active fault zones, their number, or local variations in the strain rate applied to them. Thus, although the relation suggests a useful method for evaluating seismic hazard in a plate boundary, numerical evaluation of the distribution of slip is considered desirable in any specific region. As an example, we estimated slip rates on fault zones near San Francisco Bay.

We modeled fault segments (Fig. 3) as vertical frictionless dislocations in an elastic plate of uniform thickness. The plate was subjected to antisymmetric displacements at an azimuth and rate appropriate to the inferred local plate slip vector (*18*). Boundary element methods were used to determine the amount of slip along the strike on each fault (*19*) that was required to minimize stresses in the plate. These stresses resulted from the plate boundary displacements and from the simultaneous slip of all other fault elements in the plate boundary (*11*). The calculated distribution of slip along the Calaveras and Hayward fault zones depended on the way we connected fault segments.

The plate boundary slip rate at this latitude is approximately 38 mm/year (*7*), absorbed largely by the throughgoing San Andreas fault. As the connectivity between fault segments was increased, slip rates decreased on the San Andreas fault and increased on the Hayward and Calaveras faults (Fig. 3). They increased northward on the Hayward fault zone if the Maacama, Rodgers Creek, and Hayward faults were

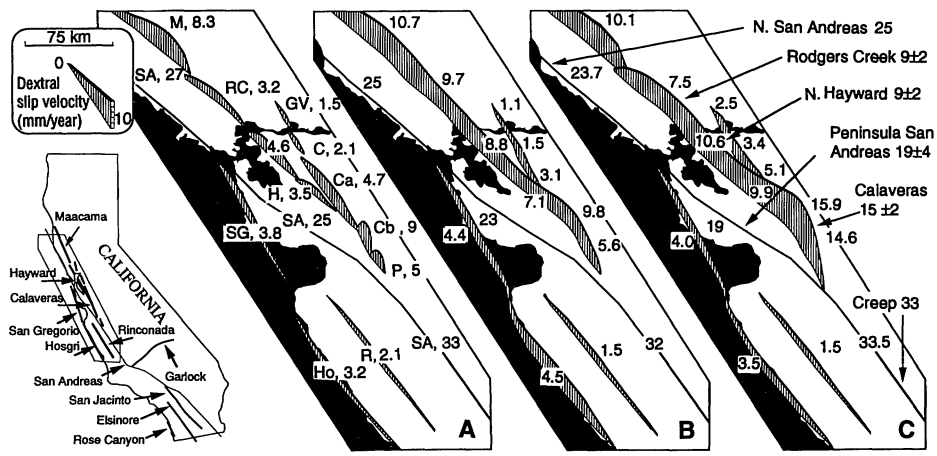

Fig. 3. California plate boundary showing fault zones and boundary element models for slip in the Bay area (inset). Faults: M, Maacama; RC, Rodgers Creek; H, Hayward; SG, San Gregorio; Ho, Hosgri; R, Rinconada; SA, San Andreas; GV, Green Valley; C, Concord; Ca, Northern Calaveras; Cb, Central Calaveras; P, Paicines. Rates on the San Andreas fault are indicated but not graphed. Slip rates lower than observed characterize the isolated faults shown in (**A**). Increased fault zone connectivity in (**B**) and (**C**) resulted in increased slip rates on the Hayward, Calaveras, and San Gregorio fault zones. The Mission fault links the Hayward and Calaveras faults. (B) and (C) differ only in the connectivity between the Maacama and Hayward fault zones and that between the Calaveras and San Andreas fault zones. Values used in estimating probabilities of large earthquakes (*1*) are indicated in the margin to the right of (C).

connected (Fig. 3B), but the maximum slip rate on the south central Maacama fault (10.7 mm/year) was larger than considered reasonable (*16*), and the maximum slip rate on the Calaveras fault (*1*) was smaller than observed (9.8 mm/year). Better agreement between model results and observed slip rate data was obtained in a model in which the Rodgers Creek, Hayward, and Calaveras faults were connected along strike and the Maacama fault slipped in isolation (Figs. 3C and 4). An extended Mission fault (*20*) was invoked to link the Hayward and Calaveras faults. To connect fault zones elsewhere, we included short hypothetical fault segments corresponding to regions of diffuse seismicity. We found that the slip rates on all the East Bay fault zones (Fig. 4) were sensitive to the length of the Maacama fault, which is estimated to be between 110 and 160 km (*21*). In models in which the Maacama fault was locked, the mean slip rate on the Hayward fault did not exceed 5 mm/year.

The models identified variations of slip rate along each fault zone that were not generally incorporated in seismic hazard estimates. High-quality estimates of slip rate have been traditionally applied uniformly to a fault segment and sometimes to a whole fault zone. For example, a slip rate of 9 ± 2 mm/year (*22*) on the southern Hayward fault has been adopted as the mean slip rate for the entire Hayward fault in revised estimates for earthquake probabilities in the Bay area. Our models suggested that this mean rate is consistent with observed slip rates on the San Andreas (*1*, *23*) and Calaveras faults but that slip rates decay from 11 ± 1 mm/year near Fremont on the Hayward fault to less than 7 mm/year near Sonoma on the Rodgers Creek fault. Slip rates on the San Gregorio zone and the Rinconada fault were less than 4 and 2 mm/year, respectively. On the San Gregorio and Hosgri faults, slip rates were not strongly sensitive to connectivity and were lower than mean published values. By contrast, the slip rate on the southern Calaveras fault was strongly sensitive to its connectivity with the San Andreas fault, as exemplified by the difference in slip rates evident in Fig. 3, B and C. The Green Valley fault has a surface creep rate higher than that predicted by our models (*24*). This may result from a surface creep transient higher than the long-term average rate or from connections of the Green Valley fault to active faulting to the northwest (*25*). Slip rates on isolated fault segments in the region not associated with the major zones that we treated are insignificant. Segments shorter than 20 km (Napa and Greenville faults) slip at rates of less than 1 mm/year. If the lengths and connectivity of these smaller faults were known precisely, data from the major fault zones could be used to infer slip rates on many active faults in the plate boundary for which slip rate data are currently unavailable.

Only a finite number of combinations of fault connectivity are possible with the fault segments shown in Fig. 3A. We have explored all combinations that seem reasonable to us. Given uncertainties in plate velocity, observed slip rate, and mapped geometry, we estimate that values in Fig. 3 are accurate to within 15%. However, our models will be inaccurate if significant fault segments remain unidentified along strike. For example, seismic data suggest that active faulting may continue in the subsurface northwest of the Green Valley fault and Maacama faults (*25*). If these faults are connected with the Calaveras and Hayward fault zones, this will result in new models in which higher slip rates occur on the Hayward and Calaveras faults at the expense of slip on the northern San Andreas fault. The boundary element model we have used to estimate relative slip rates is simplistic in that it is two-dimensional, ignores variations in elastic and frictional properties, and is immune to variations in the thickness of the elastic plate, basal traction, and the dip of faults. The inclusion of more realistic parameters (*26*) would refine estimates of slip rates in the plate boundary. However, the important features of the model are dominated by the lengths of faults, their geometries, and their interactions.

The inferred segment connectivity in the Bay area may have implications for seismic rupture. The combined lengths of the Rodgers Creek, Hayward, and southern Calaveras fault segments suggest that, were they to fail simultaneously, the resulting earthquake would be a magnitude (M)7.5 event, compared to current estimates for a maximum M7 event (*1*). A larger event (M7.7) would result from the simultaneous rupture of the Maacama fault. However, throughgoing rupture may be rare and our results do not challenge current thinking on segment-controlled rupture termination or initiation. Offsets of more than 5 km on the Anatolian fault zone appear capable of terminating rupture (*27*). The recent Landers earthquake in Southern California shows that in some circumstances a rupture may occur regardless of substantial offsets between fault segments (*28*). In addition, we consider that simultaneous rupture of the Maacama, Hayward, and Rodgers Creek faults may be possible.

Fault segment length is clearly an important factor in determining the slip rate of an isolated segment; fault segment connectivity and applied strain rate are of equal importance in determining long-term slip rates in a segmented fault zone. These rates vary along the strike of discontinuous fault zones and may be significantly modified by interactions with neighboring fault zones. It is thus inappropriate to apply point estimates of slip rate to entire fault zones as is now common practice. Once fault zone connectivity has been determined, a limited set of high-quality slip rate estimates within the fault system can be used to constrain slip rates on other faults in the system that may otherwise elude precise geologic study. Whereas the physical processes that result in connectivity between segments remain obscure, it is evident that some form of underlying mechanical linkage is responsible for the observed systematic behavior of faults in the San Francisco Bay area. The collective fault zones that constitute the California plate boundary are appropriately named the San Andreas fault system.

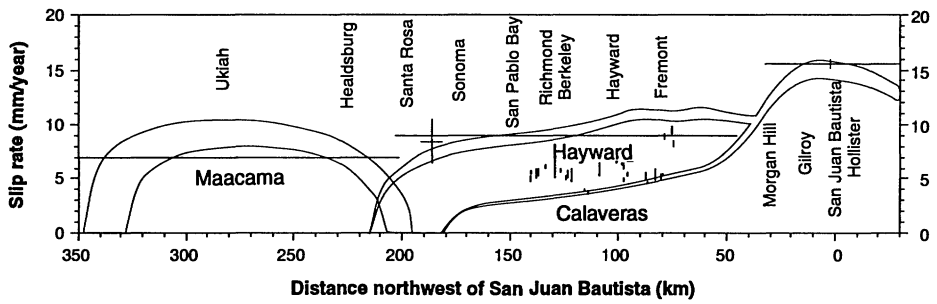

Fig. 4. Slip rates on the Hayward and Calaveras fault zones estimated with the fault connectivity in Fig. 3C. Observed values for slip are indicated by vertical lines (*22*) and by a cross (*23*). The upper limits of the outlined areas are the fault slip rates we anticipated from a Maacama fault 151 km long; the lower bounds correspond to a Maacama fault 110 km long. Long horizontal lines indicate preferred slip rates adopted by various authors for the Maacama (*16*), Hayward, and Calaveras faults (*1*).

REFERENCES AND NOTES

1. Working Group on California Earthquake Probabilities, *U.S. Geol. Surv. Circ. 1053* (1990).
2. J. N. Brune, *J. Geophys. Res.* **73**, 777 (1968).
3. K. Sieh, in *Earthquake Prediction, an International Review*, D. Simpson and P. Richards, Eds. (Maurice Ewing Series, no. 4, American Geophysical Union, Washington, DC, 1981), pp. 181–207.
4. U.S. Geological Survey Staff, *Science* **247**, 286 (1990).
5. W. Thatcher and M. Lisowski, *J. Geophys. Res.* **92**, 4771 (1987).
6. R. E. Wallace [*U.S. Geol. Surv. Prof. Pap. 1515*

(1990), p. 3] describes the San Andreas fault as a system of several major fault zones. Each comprises numerous fault segments consisting of individual faults. Geological segments are typically recognized by their geometry, but segments can be defined by their seismic rupture properties or by other geophysical characteristics common to contiguous faults of a fault zone. In (*11*) fault zones are defined in terms of contiguous straight fault segments, some of which were used in the present study. We did not consider segments smaller in length than the plate thickness (≈10 km), and we treated the Hayward, Calaveras, and San Gregorio faults as zones of groups of segments.

7. M. Lisowski, J. C. Savage, W. C. Prescott, *J. Geophys. Res.* **96**, 8369 (1991).
8. C. H. Scholz and P. A. Cowie, *Nature* **346**, 837 (1990); P. A. Cowie and C. H. Scholz, *J. Struct. Geol.*, in press.
9. C. H. Scholz, *The Mechanics of Earthquakes and Faulting* (Cambridge Univ. Press, Cambridge, 1991).
10. T. Rikitake, *Tectonophysics* **23**, 299 (1974).
11. R. Bilham and G. King, *J. Geophys. Res.* **94**, 10204 (1989); *U.S. Geol. Surv. Open-File Rep. 89-315* (1989), p. 80.
12. C. H. Jones and S. G. Wesnousky [*Science* **256**, 83 (1992)] and (*11*) quantify the effects of oblique slip near transpressional segments of the San Andreas fault system.
13. J. F. Pacheco, C. H. Scholz, L. R. Sykes, *Nature* **355**, 71 (1992); B. Romanowicz, *Geophys. Res. Lett.* **19**, 481 (1992).
14. G. C. P. King and J. Nabelek, *Science* **228**, 984 (1987); S. G. Wesnousky, *Bull. Seismol. Soc. Am.* **80**, 1374 (1990); R. H. Sibson, in *Earthquake Source Mechanics*, S. Das, J. Boatwright, C. H. Scholz, Eds. (Geophys. Monogr. 37, American Geophysical Union, Washington, DC, 1986), pp. 157–167.
15. It is common for displacements on strike-slip faults to exceed 10% of their total length (*8, 9*); S. G. Wesnousky, *Nature* **335**, 340 (1988); G. C. P. King, *Pure Appl. Geophys.* **124**, 567 (1986).
16. S. G. Wesnousky, *J. Geophys. Res.* **91**, 12,587 (1986).
17. A. J. Michael and D. Eberhart-Phillips, *Eos* **72**, 483 (1991).
18. In our model we used a transverse Mercator projection of the faults centered on the pole of rotation between the Pacific and North American plates [C. DeMets, R. G. Gordon, D. F. Argus, S. Stein, *Geophys. J. Int.* **101**, 425 (1990)].
19. S. L. Crouch and A. M. Starfield, *Boundary Element Methods in Solid Mechanics* (Allen and Unwin, London, 1989); our program was coded by G. C. P. King. Antisymmetric displacements applied to a single, vertical, frictionless fault, consisting of several contiguous elements in an elastic plate, resulted in a distribution of slip with a maximum near the center of the fault. The variation of slip along strike (in this case, elliptical in form) was evaluated numerically. The slip distribution on fault segments with complex fault geometries is discussed in (*11*). To obtain realistic slip distributions, we divided each fault zone into short straight segments (>10 km) consistent with the mapped geometry of each fault zone, and we divided each segment in the model into five or more contiguous subelements. More than 60 elements were used in some of the models.
20. D. J. Andrews, D. H. Oppenheimer, J. J. Lienkamper, *J. Geophys. Res.*, in press.
21. Surface exposures of the active Maacama fault reveal that slip is distributed over several subparallel fault strands [E. H. Pampeyan, P. W. Harsh, J. M. Coakley, *U.S. Geol. Surv. Misc. Field Stud. Map 1217* (1981)]. Although fault creep at 2 mm/year was observed on one fault strand, a value for the total Holocene slip rate is unavailable [R. R. Upp, *Eng. Geol. (Amsterdam)* **27**, 375 (1989)]. The fault was outlined by microseismicity (*25*), and in (*16*) a value of 7 mm/year was adopted for seismic hazard estimates.
22. J. L. Lienkamper, *U.S. Geol. Surv. 1:24000 Map MF 2196* (1992); ———, G. Borchardt, M. Lisowski, *J. Geophys. Res.* **96**, 18,261 (1991).
23. T. M. Niemi and N. T. Hall, *Geology* **20**, 195 (1992).
24. J. S. Galehouse, *U.S. Geol. Surv. Open-File Rep. 91-352* (1991), p. 375.
25. W. L. Ellsworth, *U.S. Geol. Surv. Prof. Pap. 1515* (1990), p. 153; D. A. Castillo and W. L. Ellsworth *J. Geophys. Res.*, in press.
26. K. P. Furlong, W. D. Hugo, and G. Zandt [*J. Geophys. Res.* **94**, 3100 (1989)] have developed sophisticated three-dimensional rheological models for northern California based on its thermal history. Their application would be useful for improved models for examining fault connectivity in the region.
27. A. A. Barka and K. Kadinsky-Kade, *Tectonics* 7, 663 (1988).
28. The 80-km-long surface rupture of the Landers earthquake included several mapped and unmapped faults (Camp Rock, Johnson Valley, and Emerson faults) that were separated by more than 5 km.
29. K. E. Budding, D. P. Schwartz, D. H. Oppenheimer, *Geophys. Res. Lett.* **18**, 447 (1991).
30. S. F. McGill and K. E. Sieh, *J. Geophys. Res.* **96**, 21597 (1991).
31. E. Hauksson, in *Engineering Geology Practice in Southern California*, B. W. Pipkin and R. J. Proctor, Eds. (Association of Engineering Geologists Spec. Publ. No. 4, Southern California Section, Star Publishing, Belmont, CA, 1992), in press.
32. Supported by the NSF.

14 April 1992; accepted 13 July 1992

Mass-Spectrometric ^{230}Th-^{234}U-^{238}U Dating of the Devils Hole Calcite Vein

Kenneth R. Ludwig,* Kathleen R. Simmons, Barney J. Szabo, Isaac J. Winograd, Jurate M. Landwehr, Alan C. Riggs, Ray J. Hoffman

The Devils Hole calcite vein contains a long-term climatic record, but requires accurate chronologic control for its interpretation. Mass-spectrometric U-series ages for samples from core DH-11 yielded ^{230}Th ages with precisions ranging from less than 1,000 years (2σ) for samples younger than ~140 ka (thousands of years ago) to less than 50,000 years for the oldest samples (~566 ka). The $^{234}U/^{238}U$ ages could be determined to a precision of ~20,000 years for all ages. Calcite accumulated continuously from 566 ka until ~60 ka at an average rate of 0.7 millimeter per 10^3 years. The precise agreement between replicate analyses and the concordance of the $^{230}Th/^{238}U$ and $^{234}U/^{238}U$ ages for the oldest samples indicate that the DH-11 samples were closed systems and validate the dating technique in general.

Core DH-11 of the Devils Hole (DH) calcite vein contains a continuous record of stable-isotopic variation in Great Basin ground water for most of the past several hundred thousand years (*1*). Spectral analyses of ^{18}O and ^{13}C records of DH-11, as well as inferences on timing of glacial-interglacial transitions (*1*), rely on the accuracy of the chronometric control. To provide this control, we determined mass-spectrometric (MS) uranium-series ages (*3*) for 21 samples across DH-11, using replicate analyses to validate estimates of uncertainty.

For each analysis, ~300 mg of calcite chips were selected for visual purity and freedom from porosity. The chips were ultrasonically cleaned, dissolved in HNO_3, spiked with ^{229}Th, ^{233}U, and ^{236}U, and purified with conventional ion-exchange methods. The purified U and Th were loaded with colloidal graphite on separate Re filaments (*3*) and analyzed in an automated mass spectrometer (*4*). To evaluate both the precision and accuracy of the dates, we examined possible sources of bias and external variance in the measurements (*5*) using instrumental checks (*6*) and two levels of replicate analyses. Thus, we have not relied on precision estimates arising solely from the internal statistics of the mass-spectrometric analyses.

The primary standard for this study was a solution of Precambrian uraninite that has been shown to be in secular equilibrium (*7*). Analyses of spiked aliquots of this standard were performed after every few samples and provide a test of the reproducibility of single analyses. The mean single-analysis precision of $^{230}Th/^{238}U$ for the secular-equilibrium standard was 0.24% (2σ, 12 analyses, no apparent external variance) (*5*, *8*). For $^{234}U/^{235}U$, a proxy for $^{234}U/^{238}U$, the mean single-analysis precision was 0.31% (2σ, 29 analyses), including a resolvable external error of 0.25% (*5*, *9*). Therefore, an additional variance corresponding to the 0.25% external error was added to the internal variance for each $^{234}U/^{235}U$ analysis. The weighted-mean

K. R. Ludwig, K. R. Simmons, B. J. Szabo, A. C. Riggs, U.S. Geological Survey, Mail Stop 963, Federal Center, Denver, CO 80225.
I. J. Winograd and J. M. Landwehr, U.S. Geological Survey, National Center, Mail Stop 432, Reston, VA 22092.
R. J. Hoffman, U.S. Geological Survey, 705 Plaza Street, Carson City, NV 89701.
*To whom correspondence should be addressed.